Interferometric Detection of Linear Polarization from Sagittarius A* at 230 GHz

Geoffrey C. Bower[1], Melvyn C.H. Wright[1], Heino Falcke[2], Donald C. Backer[1]

ABSTRACT

We measured the linear polarization of Sagittarius A* to be $7.2 \pm 0.6\%$ at 230 GHz using the BIMA array with a resolution of 3.6×0.9 arcsec. This confirms the previously reported detection with the JCMT 14-m antenna. Our high resolution observations demonstrate that the polarization does not arise from dust but from a synchrotron source associated with Sgr A*. We see no change in the polarization position angle and only a small change in the polarization fraction in four observations distributed over 60 days. We find a position angle 139 ± 4 degrees that differs substantially from what was found in earlier JCMT observations at the same frequency. Polarized dust emission cannot account for this discrepancy leaving variability and observational error as the only explanations. The BIMA observations alone place an upper limit on the magnitude of the rotation measure of 2×10^6 rad m^{-2}. These new observations when combined with the JCMT observations at 150, 375 and 400 GHz suggest RM $= -4.3 \pm 0.1 \times 10^5$ rad m^{-2}. This RM may be caused by an external Faraday screen. Barring a special geometry or a high number of field reversals, this RM rules out accretion rates greater than $\sim 10^{-7}$ M$_\odot$ y^{-1}. This measurement is inconsistent with high accretion rates necessary in standard advection dominated accretion flow and Bondi-Hoyle models for Sgr A*. It argues for low accretion rates as a major factor in the overall faintness of Sgr A*.

Subject headings: Galaxy: center — galaxies: active — polarization — radiation mechanisms: non-thermal — scattering

---

[1]Astronomy Department & Radio Astronomy Laboratory, University of California, Berkeley, CA 94720; gbower,wright,dbacker@astro.berkeley.edu

[2]Max Planck Institut für Radioastronomie, Auf dem Hügel 69, D 53121 Bonn Germany; hfalcke@mpifr-bonn.mpg.de

1. Introduction

Linear and circular polarization are important diagnostics of synchrotron sources. In active galactic nuclei and galactic microquasars, polarization is useful for characterizing particle energy, magnetic field configuration and jet composition (Marscher & Gear 1985; Wardle et al. 1998; **?**). Variability in polarization is important for diagnosing shocks and the stability of accretion processes.

Here we present new observations of linear and circular polarization in Sagittarius A*, the compact nonthermal radio source in the Galactic Center. Sgr A* is associated with a $3 \times 10^6 M_\odot$ black hole (Melia & Falcke 2001). While much is known about this source, there is still dispute over the nature of accretion and outflow in the source. Advection dominated accretion flows (ADAFs), convection dominated accretion flows (CDAFs), Bondi-Hoyle accretion, Blandford-Königl-type jets and hybrids of these ideas have been used to characterize the spectrum and size of Sgr A* (e.g., Narayan et al. 1998; Quataert & Gruzinov 2000; Liu & Melia 2001; Falcke & Markoff 2000; Yuan et al. 2002). In general models account for the low luminosity of Sgr A* through a very low accretion rate, through a very low radiative efficiency or through a combination of these. Estimates of the accretion rate vary by seven orders of magnitude. Linear polarization observations can break this degeneracy.

These new observations complement past work that has shown a complex picture of the polarization in Sgr A*. The emission shows no linear polarization between 1.4 and 112 GHz at limits of 0.1 to 2% (Bower et al. 1999a,c, 2001b). Surprisingly, the emission is circularly polarized between 1.4 and 43 GHz (Bower et al. 1999b; Sault & Macquart 1999; Bower et al. 2002a). The circular polarization is strong and variable, sometimes showing a highly inverted spectrum. Models account for the circular polarization and absence of linear polarization through conversion of linear to circular polarization and bandwidth depolarization of the linear polarization with cold electrons (Ruszkowski & Begelman 2002; Beckert & Falcke 2002). A model that involves plasma modes in the vicinity of a black hole has also been developed (Broderick & Blandford 2000).

The polarization properties above 112 GHz are less certain. JCMT observations at 150, 220, 375 and 400 GHz (2.0, 1.35, 0.85 and 0.75 mm wavelength, respectively) indicate that Sgr A* is polarized at a level of $\sim 10\%$ (Aitken et al. 2000, hereafter A00). However, these observations suffer from the poor angular resolution of the JCMT ($22''$ at 220 GHz). A substantial amount of polarized and unpolarized radiation must be subtracted from the flux detected at the Galactic Center to estimate the polarization of Sgr A*. The apparent sharp transition in linear polarization apparent between 112 and 150 GHz from these observations is very unusual and has important implications for the source physics (Quataert & Gruzinov 2000; Agol 2000; Melia et al. 2000).

We present interferometric observations of the linear polarization in Sgr A* at 230 GHz (1.3 mm wavelength). Made with the BIMA array, these observations are approximately two orders of magnitude higher resolution than those of the JCMT. Thus, we are able to eliminate the effects of extended polarized and unpolarized emission and isolate the emission of Sgr A* itself. We present the observations in §2, discuss the results in §3 and summarize in §4.

2. Observations and Data Reduction

Data were obtained on 4 epochs (Table 1) in the B and C configurations of the BIMA array (Welch et al. 1996). The measured single sideband system temperature on Sgr A* ranged from 1000 to 2800 K for the B-configuration data, and 1500 to 9000 K for the C-configuration data. Both upper (230.7 GHz) and lower sideband (227.3 GHz) were sampled with a bandwidth of 800 MHz. The data were obtained from switched polarization observations (see Bower et al. 1999c). The polarization on each antenna is switched between left and right circular polarization (L and R) using a Walsh switching pattern of period 16. Using an integration time of 11 second, all polarization combinations (LL, RR, LR and RL) are sampled every 5 minutes.

The data were phase self-calibrated by using the LL and RR polarizations averaged over 5 minutes. Phase calibration was applied to all 4 polarizations LL, RR, LR, and RL. Amplitude calibration of the BIMA array is determined from measurements of the antenna gains (~ 150 Jy K^{-1}) using planet observations at a number of epochs. The antenna gains are stable and no further amplitude calibration was applied.

The observed amplitudes are sensitive to atmospheric coherence and to antenna pointing errors. Both errors affect polarized and unpolarized emission equally, implying that the polarization fractions are a more reliable measurement than the total or polarized intensities. The antenna pointing was checked on the quasar J1733-1304 and Uranus. We estimate the magnitude of these errors from measurements of the flux density for J1733-1304 in February through May 2002. The measurements are 2.2 ± 0.2 Jy at 0.85 mm (JCMT); 2.3 ± 0.3 (BIMA) and 3.0 ± 0.3 (OVRO), at 1.3 mm; and, 4.3 ± 0.3 (BIMA) and 3.7 ± 0.3 (OVRO) at 3 mm (B. Matthews and J. Carpenter, private communication). These are consistent with a coherence loss $< 30\%$ for our 1.3 mm polarization measurements.

Polarization calibration was applied using the polarization leakage terms derived from observations in the same mode of 3C 273 and 3C 279 on 02 February 2002. The polarization leakage for each antenna ranges from ~ 1 to 5% on all but one antenna. The polarization results for Sgr A* were identical with and without antenna 8, which had leakage terms $\sim 10\%$. Comparison of the polarization calibrations in 8 epochs over the past 1.5 years shows that the leakage terms are stable and reproducible to $\sim 1.5\%$ rms (Bower et al. 2002b). This leads to a random systematic error in the polarization of $\sim 0.5\%$.

We compared the polarized flux density for 3C 279 measured with BIMA at 86 and 230 GHz and measured with the VLA at 22 and 43 GHz over the past 2 years (Taylor & Myers 2000; Bower et al. 2002b). The fractional polarization shows the same behavior from 22 to 230 GHz. The VLA and BIMA position angles differ by ~ 10 degrees. It is not known whether this difference is due to source structure or an intrinsic error in the VLA or BIMA calibration.

The polarization leakage corrections were applied by averaging the switched polarization data over intervals ranging from 2 to 30 minutes. We calibrated upper and lower sideband observations separately for each epoch. The errors in the polarization were consistent with the thermal noise for averaging times from 5 to 30 minutes.

Combining all the data weighted by system temperature and spatially filtered to include only (u,v)-data between 20 and 300 $k\lambda$, we obtain the images shown in Figure 1. With robust weighting to minimize the noise from sidelobes and thermal noise we obtain a synthesized beamwidth 3.6 x 0.9 arcsec with a theoretical rms noise level 10 mJy. We combined the data in several combinations to look for changes in the polarization with time, frequency and array configuration. The results are summarized in Table 2. Fluxes were found by fitting point sources at the center of the field. LSB and USB refer to the lower and upper sideband data sets including all epochs. B, C1, C2 and C3 refer to the four epochs summarized in Table 1. C refers to a combination of all three C-configuration observations. For the combined result, we find the linear polarization to be $7.2 \pm 0.6\%$ in position angle 139 ± 4 degrees.

3. Discussion

3.1. Dust Polarization

These observations confirm the existence of high fractional linear polarization in or near Sgr A* at 230 GHz. They can be used to eliminate the possibility of dust contamination of the polarized signal. A00 estimated that their central $22''$ beam included 3.55 Jy of (unpolarized) free-free emission and 0.75 Jy of dust emission at 220 GHz which left 2.2 ± 0.5 Jy for Sgr A*. A00 assume that the dust emission is 3% polarized at a position angle of 100 degrees based on the larger scale properties of the dust polarization. If we assume that the dust and free-free emission are distributed smoothly over this beam, then we expect a factor of $\frac{22\times22}{3.6\times0.9} = 150$ decrease in these flux densities for the BIMA result. Thus, even 100% polarized dust emission could produce only ~ 5 mJy of the observed 89 mJy of polarized flux density.

Could the dust be significantly clumped to produce the observed polarization? If all of the dust emission were concentrated in our central pixel, then the minimum dust polarization fraction is $\sim 12\%$. However, this leaves only 0.5 Jy flux density for Sgr A* itself, which is very low given the known spectrum and history of millimeter flux density observations. The minimum flux density observed for Sgr A* at 1.3 mm is > 1 Jy (Zhao et al. 2002). Introducing a decorrelation factor $\xi \leq 1$ gives a flux density of $0.5\xi^{-1}$ Jy for Sgr A* and a dust polarization fraction $12\xi^{-1}\%$. Our limit on gain errors derived from J1733-1304 places the constraint $\xi > 0.7$, which doesn't substantially increase the flux density for Sgr A*. Interferometric observations of dust polarization indicate that dust polarization rarely exceeds 20% and only in cases of dense star-forming molecular clouds (Rao et al. 1998; Lai et al. 2002). An unlikely coincidence would be necessary to place such a rare, highly clumped and highly polarized cloud at the location of Sgr A*.

We conclude therefore that the effects of dust polarization on our measurement are negligible and that the emission is associated with Sgr A* itself.

3.2. Variations with Wavelength and Time

While the polarization fraction we measured agrees with that of A00, the position angle of 139 ± 4 degrees does not. A00 measured a total polarization of 4.1% (266 mJy) in position angle 89 ± 3 degrees in the central pixel at 220 GHz. Some of this polarized emission is dust which A00 assume to be polarized at 3% (25 mJy) in position angle 100 degrees. We can estimate the actual dust parameters necessary to make our measurements agree. Since our measured Sgr A* polarization is almost orthogonal in (Q, U)-space to the central pixel of A00, the required dust polarization for agreement is extreme: 300 mJy (or 40% of the estimated 750 mJy of dust flux density) in position angle 80 degrees. This high polarization fraction is inconsistent with other measured polarization fractions as discussed above. Thus, we cannot easily reconcile the A00 220 GHz result with ours through the dust properties.

We can estimate the rotation measure from the position angle data as a function of frequency (Figure 2). The lack of bandwidth depolarization in the BIMA results places a strong upper limit of $\sim 10^8$ rad m^{-2} on the RM. The LSB and USB results for BIMA are nearly identical, placing an upper limit of 2×10^6 rad m^{-2}. The best fit to these data points is -3×10^5 rad m^{-2} but the error is $> 10^6$ rad m^{-2}. Although we can reconcile all the BIMA and JCMT position angles with RM $\sim -3 \times 10^6$ rad m^{-2} and three phase wraps between 150 and 400 GHz, a RM this large would lead to substantial depolarization in the broad (40 GHz) JCMT bandpasses. We would expect to find a much higher polarization fraction in the BIMA results which have much narrower bandpasses. In fact, based on the nearly equal polarization fractions in the BIMA and JCMT results, we can conclude again that the polarization must be $< 10^6$ rad m^{-2}.

However, if we exclude the A00 220 GHz result, we find that all of the remaining polarization detections can be explained as the result of a single RM without leading to substantial depolarization. We measure RM $= -4.3 \pm 0.1 \times 10^5$ rad m^{-2} and a zero-wavelength position angle of 181 ± 2 degrees. Including the A00 220 GHz result gives $-4.3 \times 1.6 \times 10^5$ rad m^{-2}. This error could be construed as including the effects of systematic measurement error and variability. If we exclude both the 150 and 220 GHz A00 result, we find RM $= -4.4 \pm 0.4 \times 10^5$ rad m^{-2}. While the exclusion of the low frequency JCMT points in the RM fit appears *ad hoc*, note that these are the least reliable of the JCMT results due to the much larger beam size. Nevertheless, this RM measurement must be considered tentative.

We cannot eliminate variability as an explanation for the differences in position angle that are seen. The A00 results were obtained in three separate epochs spread over 5 months nearly three years earlier than the BIMA results. However, we detect no change in the position angle of the linear polarization with time in the BIMA data (Figure 3). The reduced χ^2 is 0.5 for the four epochs under the hypothesis of a constant position angle. Further, the A00 measurements at 375 and 400 GHz were separated by 5 months but show no apparent change. On the other hand, the fractional linear polarization in the BIMA data is slightly variable. The final epoch C3 is significantly different from the mean. The reduced χ^2 is 2.0 for the four epochs under the hypothesis of a constant polarization.

We summarize detections and upper limits for the linear polarization fraction in Figure 4. There is a sharp transition in the polarization fraction between 100 and 200 GHz. Our previous BIMA measurement that led to an upper limit at 112 GHz cannot be explained by bandwidth depolarization. Bandwidth depolarization occurs at 112 GHz in 800 MHz of bandwidth when RM $> 1.0 \times 10^7$ rad m^{-2}.

On the other hand, angular depolarization, which requires that the RM change the position angle by > 180 degrees across the face of the source, is marginally adequate. At 112 GHz, an RM a few times 10^5 rad m^{-2} is just sufficient. Thus, a fully turbulent accretion region with an outer scale comparable to the source size ($<$ 1AU, see discussion below) could depolarize the source. However, measured RM flucutuations in the Galactic Center and Cygnus regions have a maximum of $< 10^3$ rad m^{-2} on degree scales and are $<< 1$ rad m^{-2}

when extrapolated to scales below 1 arcsec (Lazio et al. 1990; Yusef-Zadeh et al. 1997). Nevertheless, turbulence in the accretion environment may be substantially different from that in the interstellar medium.

An alternative explanation is that Sgr A* consists of an unpolarized source and a polarized source with a steeply inverted spectrum that dominates the spectrum above 230 GHz. A two component model is natural for both inflow and outflow models since they must account for the sharply increasing spectrum at millimeter wavelengths (Serabyn et al. 1997; Falcke et al. 1998). All models (see next section) that fit the centimeter to submillimeter spectrum include at least two distinct populations of radiating particles. If the spectrum rises as $\nu^{2.5}$, then the source would depolarize by a factor of 0.16 between 230 and 112 GHz, which is sufficient to account for the absence of detection at 112 GHz. Spectral indices of < 1 and > 4 are excluded by the results.

3.3. Circular Polarization

Circular polarization is not detected in any of these data sets. For the cumulative data set the circular polarization is less than the thermal rms noise of $\sim 1\%$. Only in the B array data is there a hint of a detection. Here the circular polarization is two times the noise.

3.4. Origin and Propagation of the Linear Polarization

The maximum observed RM in the Galactic Center is on the order of a few times 10^3 rad m^{-2} (Yusef-Zadeh et al. 1997). However, this occurs in a nonthermal filament approximately 0.5 degrees away from Sgr A* and may not probe the densest ionized regions towards the Galactic Center. A hyperstrong interstellar scattering screen significantly broadens the image of Sgr A* at all wavelengths (Lo et al. 1998; Lazio & Cordes 1998; Bower et al. 2001a). The physical parameters of this scattering screen are not fully constrained. However, we can estimate an upper limit to the RM of the screen. The maximum RM is $\sim 10^4$ rad m^{-2} for models of the ionized surfaces of molecular clouds (Yusef-Zadeh et al. 1994; Lazio & Cordes 1998; Bower et al. 1999a). However, the RM may arise in a region different from the scattering region. Sgr A* is embedded in or behind Sgr A West as well as a dense, ionized halo that extends over $\sim 5'$ (Pedlar et al. 1989; Anantharamaiah et al. 1999). This halo has density of $10^2 - 10^3$ cm^{-3} and a scale of 10 pc. For magnetic field strengths of a milliGauss, the maximum RM is $\sim 10^7$ rad m^{-2}. Similarly, Sgr A West has a density 10^2 cm^{-3}, a scale of 1 pc and milliGauss field strength, giving a maximum RM

$\sim 10^5$ rad m^{-2}. Thus, while the interstellar scattering screen does not contribute significantly to the measured RM, material which closer to Sgr A* but not directly associated with accretion and outflow could.

Millimeter VLBI observations require a size for Sgr A* of 72 gravitational radii or less at 43 GHz and sizes decreasing as $\sim \nu^{-1}$ at higher frequencies (Bower & Backer 1998; Lo et al. 1998; Krichbaum et al. 1998; Doeleman et al. 2001). Theoretical temperature profiles indicate that the emission comes from a volume within a few gravitational radii of Sgr A* (Melia & Falcke 2001). In ADAF or CDAF models, the 230 GHz source is embedded within a quasi-spherical accretion region. Imaging by Chandra at X-ray wavelengths indicate that Sgr A* is extended on a scale consistent with the radius of this larger region, suggesting a concentration of hot thermal plasma (Baganoff et al. 2001b).

The emission must propagate through the accretion region without substantial depolarization. Using the measured RM $\sim -4 \times 10^5$ rad m^{-2}, we can estimate the accretion rate. (Note that the following conclusions also hold for the upper limit RM of 2×10^6 rad m^{-2} determined from the BIMA data). The implied accretion rates differ between models because of the different temperature versus radius relations. We can calculate the Bondi-Hoyle accretion rate assuming equipartition and a uniform magnetic field equation (5) from Bower et al. (1999a). To produce the measured RM, the accretion rate must be 10^{-7} M$_\odot$ y^{-1}. However, this accretion rate is too low to produce the observed spectrum by two orders of magnitude for both the ADAF and Bondi-Hoyle models. An accretion rate of 10^{-5} M$_\odot$ y^{-1} for these models can model the spectrum but requires an RM $\sim 10^{10}$ rad m^{-2}. On the other hand, CDAF models can model the spectrum with $\dot{M} \sim 10^{-8}$ M$_\odot$ y^{-1}, which produces RM $\sim 10^6$ rad m^{-2} (Quataert & Gruzinov 2000). Jet models require an accretion rate of 10^{-8} M$_\odot$ y^{-1}, which is consistent with a low RM (Falcke & Markoff 2000). Melia et al. (2000) predict 10^{-11} M$_\odot$ y^{-1}, which significantly underpredicts the RM. This model requires that the RM originates external to Sgr A*.

Two effects may mitigate the conclusions discussed above. These are magnetic field reversals and deviations from equipartition between particle and magnetic field energy. If the magnetic field reverses frequently, then the rms field in the region is a better indicator of the characteristic field for a RM calculation (Ruszkowski & Begelman 2002). A model predicting a high RM for a uniform field may produce an RM lower by orders of magnitude if there are many field reversals. However, the number of field reversals necessary to account for the difference between the ADAF or Bondi-Hoyle models and our measured RM is on the order of 10^8, which is extreme. Reducing the magnetic field strength substantially below equipartition values will reduce the RM by the same factor. However, these reductions will be offset by the necessary increase in particle density to model the same spectrum.

In jet models, the emission originates in a region of similar scale that can be located an arbitrary distance from the black hole. Jet emission is likely to originate in a compact shocked component near the base of the jet (Yuan et al. 2002). The compressed magnetic field will be perpendicular to the axis of the jet, implying that the jet is oriented North-South. Increasing magnetic field order towards the base of the jet can account for the sharply increasing polarization fraction with frequency. High frequency VLBI observations of quasars and BL Lac objects indicate that electric vector position angles are typically but not always aligned with the jet axis (Lister 2001). The inclination angle of a jet in Sgr A* is not well-constrained. However, an angle close to the line of sight is possible given that highly inclined sources often produce the highest linear polarization in compact radio sources. This raises the possibility that the radio/millimeter emission is relativistically beamed, which may also account for the absence of a visible jet or ejected components despite strong variability (e.g., Bower & Backer 1998).

The jet model does not require propagation through the accretion medium. However, the high value for the RM suggests that it may pass through some of the accretion or outflow medium (Beckert & Falcke 2002). In AGN cores, the maximum RMs measured are on the order of 2000 rad m^{-2} (Taylor 2000). This argues that we are probing a region in Sgr A* quite different from that in other AGN.

The RM we measure is not inconsistent with a lower limit for the RM from spectropolarimetry at 4.8 and 8.4 GHz (Bower et al. 1999a). No linear polarization was detected for RMs as high as 10^7 rad m^{-2} in this experiment. Different source physics may account for the absence of polarization at the longer wavelengths. This will result if the lower frequency source is intrinsically depolarized due to greater internal field disorder, for example. Alternatively, foreground beam depolarization across the much larger lower frequency source may account for the absence of linear polarization.

3.5. Predictions for Future Observations

An important expectation of emission from a jet is variable linear polarization (Marscher & Gear 1985). Variable polarization may also be a measure of the stability of accretion in a disk model. For example, **?**) have suggested that precession of the disk on a timescale of 100 days is a consequence of a very low value for the spin of the black hole. Such precession could lead to a change in the position angle of the polarization if the disk orientation is linked to the magnetic field structure. We have not seen convincing evidence for this position angle variation yet, except perhaps in the discrepancy between A00 and our result. Significant variability in the total intensity at centimeter, millimeter, submillimeter and X-ray wavelengths on timescales of hours to years has been reported (Wright & Backer 1993; Young et al. 2001; Baganoff et al. 2001a; Zhao et al. 2001; Bower et al. 2002a). Correlating polarization variability with these events could be an important clue to the origin of the polarization. However, the stable polarization that we have measured over 60 days and that A00 measured over 5 months between 375 and 400 GHz suggests that such connections are possibly subtle or require intensive monitoring. If changes in the polarization are associated with X-ray flares, then they may have a timescale of hours.

The detection of a RM and a power law index for the polarization fraction can be tested with observations at other wavelengths. BIMA observations can be spread more widely over frequency space. The 1.3 mm receivers are sensitive from 210 to 270 GHz. With properly calibrated quarter wave plates, BIMA could measure the expected difference in position angle of ~ 20 degrees over this range. BIMA can also measure differences in the power law index for the polarization fraction over this same range. Interferometric 150 GHz observations should see a substantially decreased polarization fraction but a significantly different polarization angle than observed at 230 GHz. Higher frequency observations may see the polarization fraction continue to increase.

Variability in the RM can be used as a diagnostic of the accretion or outflow medium. Sgr A* shows variability on all timescales from hours to years at radio wavelengths (Zhao et al. 2001; Bower et al. 2002a). This variability may be indicative of changes in the accretion or outflow rates or conditions, which may be reflected in the RM. Refractive scintillation timescales are on the order of 1 month at 230 GHz for a velocity of 100 $\mathrm{km s^{-1}}$.

The detection of linear polarization raises the possibility of polarimetric VLBI. Images made at 230 GHz or higher frequencies will be only weakly affected by scattering and may show the effects of general relativity (Falcke et al. 2000; Broderick & Blandford 2000; Bromley et al. 2001). This may be the best probe of the close environment of a black hole available.

4. Conclusions

We have confirmed the existence of strong linear polarization at millimeter wavelengths in Sgr A* with high resolution observations by the BIMA array. These eliminate the possibility of confusion from polarized dust emission. The polarized emission probably comes from within 10 gravitational radii of the black hole. This is one of the closest probes of the environment of a black hole that exists.

Propagation of the polarized radiation through the accretion and outflow media provides important limits on the physical characteristics in these regions. The measured RM appears to favor a very low accretion rate which excludes standard ADAF models and Bondi-Hoyle models with very high accretion rates for Sgr A*.

The existence of linear polarization at these high frequencies opens up several new methods for investigation of this source. Variations in polarization angle and fraction as well as rotation measure may provide critical constraints on models. Very long baseline interferometric imaging of linearly polarized emission in the vicinity of the black hole may reveal a wealth of effects, including those of general relativity.

The BIMA array is operated by the Berkeley-Illinois-Maryland Association under funding from the National Science Foundation.

REFERENCES

Agol, E. 2000, ApJ, 538, L121

Aitken, D. K., Greaves, J., Chrysostomou, A., Jenness, T., Holland, W., Hough, J. H., Pierce-Price, D., & Richer, J. 2000, ApJ, 534, L173

Anantharamaiah, K. R., Pedlar, A., & Goss, W. M. 1999, in ASP Conf. Ser. 186: The Central Parsecs of the Galaxy, 422

Baganoff, F. K., Bautz, M. W., Brandt, W. N., Chartas, G., Feigelson, E. D., Garmire, G. P., Maeda, Y., Morris, M., Ricker, G. R., Townsley, L. K., & Walter, F. 2001a, Nature, 413, 45

Baganoff, F. K., Bautz, M. W., Ricker, G. R., Brandt, W. N., Feigelson, E. D., Garmire, G. P., Townsley, L. K., Maeda, Y., & Morris, M. 2001b, BAAS, 199, #85.03

Beckert, T. & Falcke, H. 2002, A&A, 388, 1106

Bower, G. C. & Backer, D. C. 1998, ApJ, 496, L97

Bower, G. C., Backer, D. C., & Sramek, R. A. 2001a, ApJ, 558, 127

Bower, G. C., Backer, D. C., Zhao, J. H., Goss, M., & Falcke, H. 1999a, ApJ, 521, 582

Bower, G. C., Falcke, H., & Backer, D. C. 1999b, ApJ, 523, L29

Bower, G. C., Falcke, H., Sault, R. J., & Backer, D. C. 2002a, ApJ, 571, 843

Bower, G. C., Wright, M. C. H., Backer, D. C., & Falcke, H. 1999c, ApJ, 527, 851

Bower, G. C., Wright, M. C. H., Falcke, H., & Backer, D. C. 2001b, ApJ, 555, L103

Bower, G. C., Wright, M. C. H., & Forster, J. R. R. 2002b, BIMA Memos, 89

Broderick, A. & Blandford, R. D. 2000, BAAS, 197, #83.15

Bromley, B. C., Melia, F., & Liu, S. 2001, ApJ, 555, L83

Doeleman, S. S., Shen, Z.-Q., Rogers, A. E. E., Bower, G. C., Wright, M. C. H., Zhao, J. H., Backer, D. C., Crowley, J. W., Freund, R. W., Ho, P. T. P., Lo, K. Y., & Woody, D. P. 2001, AJ, 121, 2610

Falcke, H., Goss, W. M., Matsuo, H., Teuben, P., Zhao, J., & Zylka, R. 1998, ApJ, 499, 731

Falcke, H. & Markoff, S. 2000, A&A, 362, 113

Falcke, H., Melia, F., & Agol, E. 2000, ApJ, 528, L13

Fender, R. P., Rayner, D., McCormick, D. G., Muxlow, T. W. B., Pooley, G. G., Sault, R. J., & Spencer, R. E. 2002, MNRAS, 336, 39

Krichbaum, T. P., Graham, D. A., Witzel, A., Greve, A., Wink, J. E., Grewing, M., Colomer, F., de Vicente, P., Gomez-Gonzalez, J., Baudry, A., & Zensus, J. A. 1998, A&A, 335, L106

Lai, S., Crutcher, R. M., Girart, J., & Rao, R. 2002, ApJ, 566, 925

Lazio, T. J., Spangler, S. R., & Cordes, J. M. 1990, ApJ, 363, 515

Lazio, T. J. W. & Cordes, J. M. 1998, ApJ, 505, 715

Lister, M. L. 2001, ApJ, 562, 208

Liu, S. & Melia, F. 2001, ApJ, 561, L77

—. 2002, ApJ, 573, L23

Lo, K. Y., Shen, Z. Q., Zhao, J. H., & Ho, P. T. P. 1998, ApJ, 508, L61

Marscher, A. P. & Gear, W. K. 1985, ApJ, 298, 114

Melia, F. & Falcke, H. 2001, ARA&A, 39, 309

Melia, F., Liu, S., & Coker, R. 2000, ApJ, 545, L117

Narayan, R., Mahadevan, R., Grindlay, J. E., Popham, R. G., & Gammie, C. 1998, ApJ, 492, 554

Pedlar, A., Anantharamaiah, K. R., Ekers, R. D., Goss, W. M., van Gorkom, J. H., Schwarz, U. J., & Zhao, J. 1989, ApJ, 342, 769

Quataert, E. & Gruzinov, A. 2000, ApJ, 545, 842

Rao, R., Crutcher, R. M., Plambeck, R. L., & Wright, M. C. H. 1998, ApJ, 502, L75

Ruszkowski, M. & Begelman, M. C. 2002, ApJ, 573, 485

Sault, R. J. & Macquart, J.-P. 1999, ApJ, 526, L85

Serabyn, E., Carlstrom, J., Lay, O., Lis, D. C., Hunter, T. R., & Lacy, J. H. 1997, ApJ, 490, L77

Taylor, G. B. 2000, ApJ, 533, 95

Taylor, G. B. & Myers, S. T. 2000, VLBA Sci. Memos, 26

Wardle, J. F. C., Homan, D. C., Ojha, R., & Roberts, D. H. 1998, Nature, 395, 457

Welch, W. J., Thornton, D. D., Plambeck, R. L., Wright, M. C. H., Lugten, J., Urry, L., Fleming, M., Hoffman, W., Hudson, J., Lum, W. T., Forster, J. . R., Thatte, N., Zhang, X., Zivanovic, S., Snyder, L., Crutcher, R., Lo, K. Y., Wakker, B., Stupar, M., Sault, R., Miao, Y., Rao, R., Wan, K., Dickel, H. R., Blitz, L., Vogel, S. N., Mundy, L., Erickson, W., Teuben, P. J., Morgan, J., Helfer, T., Looney, L., de Gues, E., Grossman, A., Howe, J. E., Pound, M., & Regan, M. 1996, PASP, 108, 93+

Wright, M. C. H. & Backer, D. C. 1993, ApJ, 417, 560

Young, K. H., Zhao, J., McGary, R. S., Ho, P. T. P., Tsutsumi, T., Goss, W. M., Bower, G. C., & SMA Team. 2001, BAAS, 199, 0+

Yuan, F., Markoff, S., & Falcke, H. 2002, A&A, 383, 854

Yusef-Zadeh, F., Cotton, W., Wardle, M., Melia, F., & Roberts, D. A. 1994, ApJ, 434, L63

Yusef-Zadeh, F., Wardle, M., & Parastaran, P. 1997, ApJ, 475, L119

Zhao, J., Bower, G. C., & Goss, W. M. 2001, ApJ, 547, L29

Zhao, J.-H., Young, K. H., McGary, R. S., Ho, P. T. P., Tsutsumi, T., Lo, K. Y., Goss, W. M., & Bower, G. C. 2002, ApJ, submitted

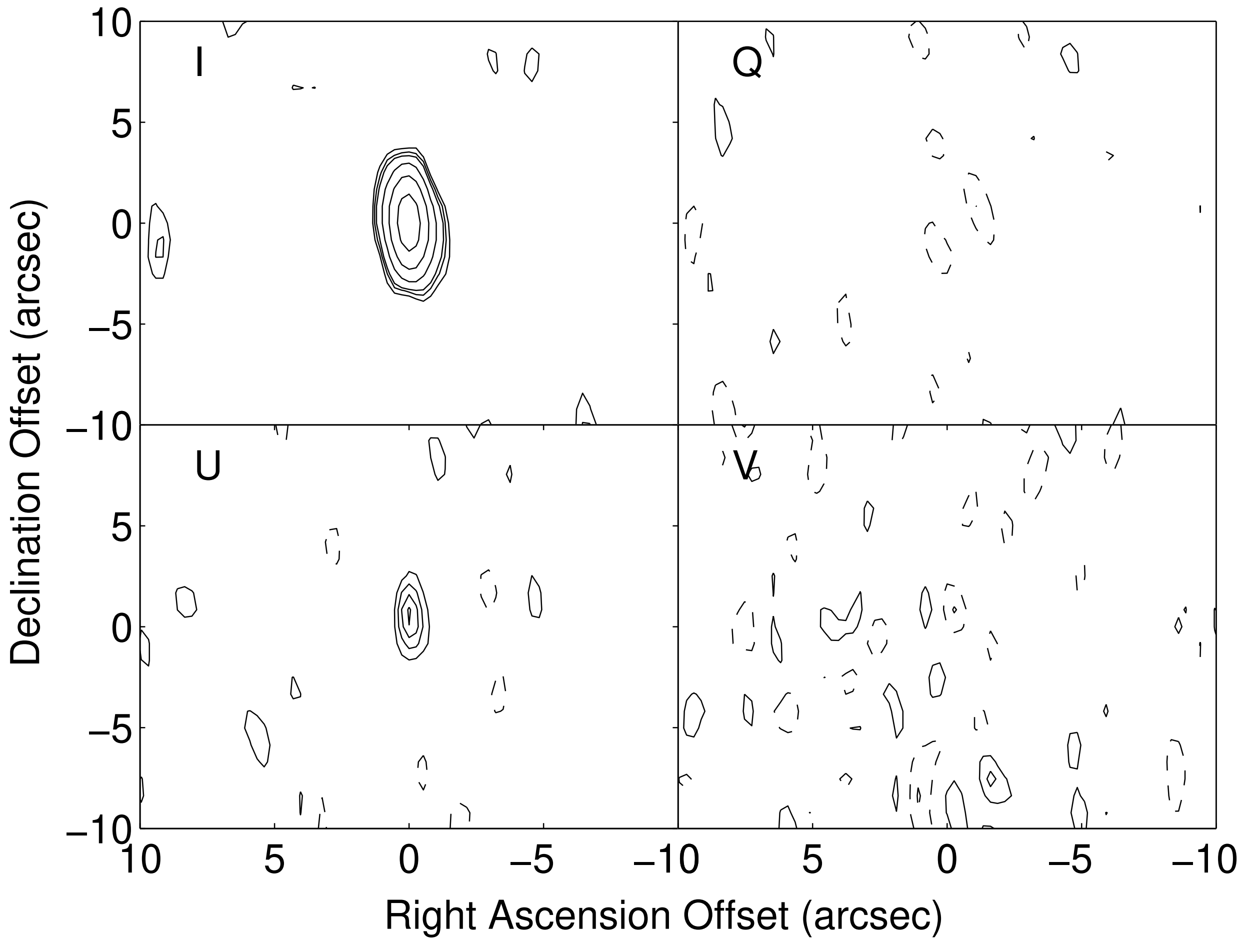

Fig. 1.— Image of Sgr A* in Stokes I, Q, U and V from the combined data set of all observations. The synthesized beam is 3.6 by 0.9 arcsec. Contours are 2, 4, 6 and 8 times the rms noise of 11 mJy beam^{-1} in the Q, U and V images. In the polarization images, positive and negative contours are shown as dashed and solid lines, respectively. Contours are shown as solid lines at 4, 6, 8, 16, 32, and 64 times 11 mJy beam^{-1} in the I image.

This preprint was prepared with the AAS LaTeX macros v5.0.

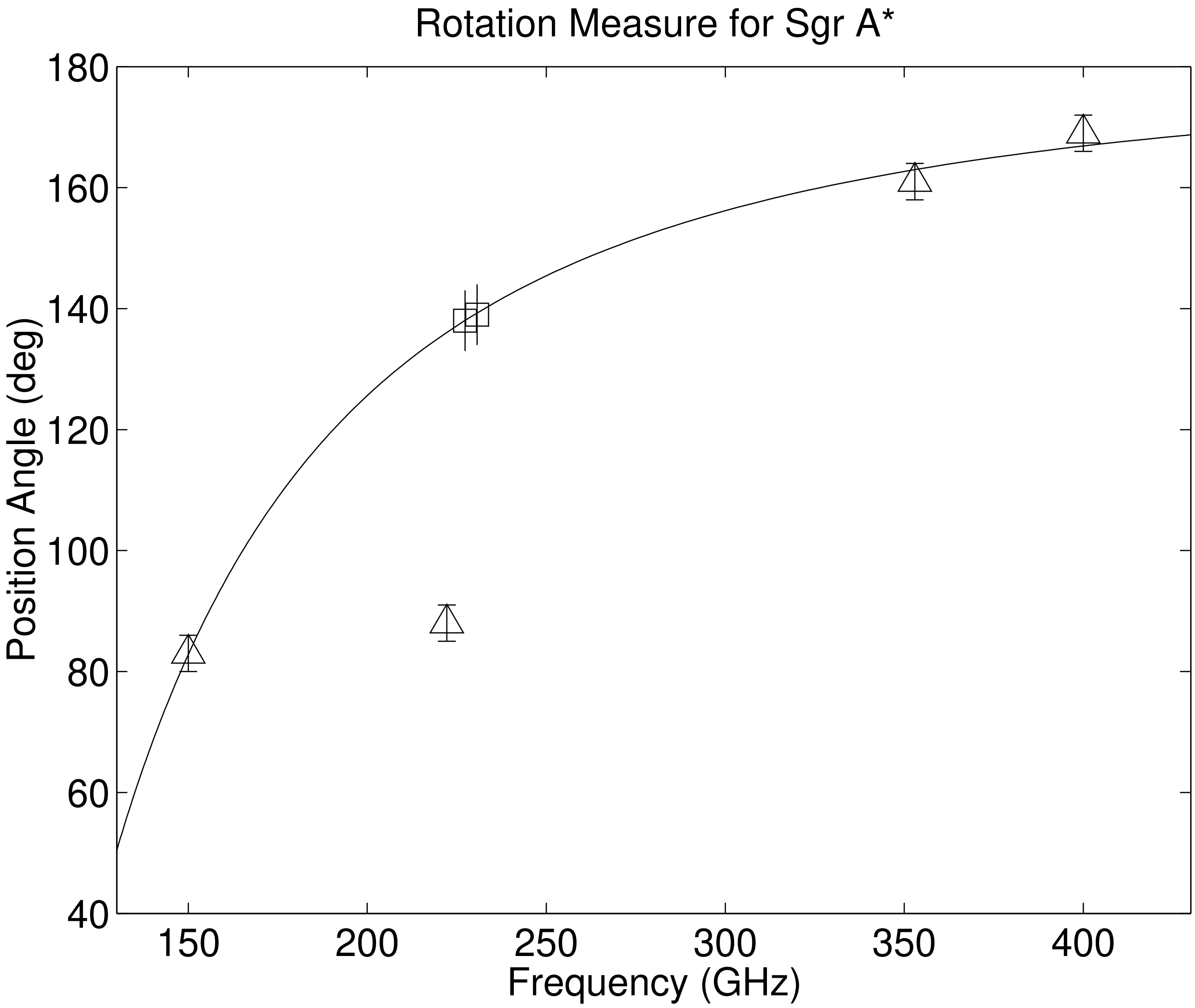

Fig. 2.— Position angle as a function of frequency. Triangles are the A00 data. Squares are the BIMA data. The solid line is a fit for the RM excluding the A00 230 GHz result. The best fit is $-4.3 \pm 0.1 \times 10^5$ rad m^{-2} with a zero-wavelength position angle of 181 ± 2 degrees.

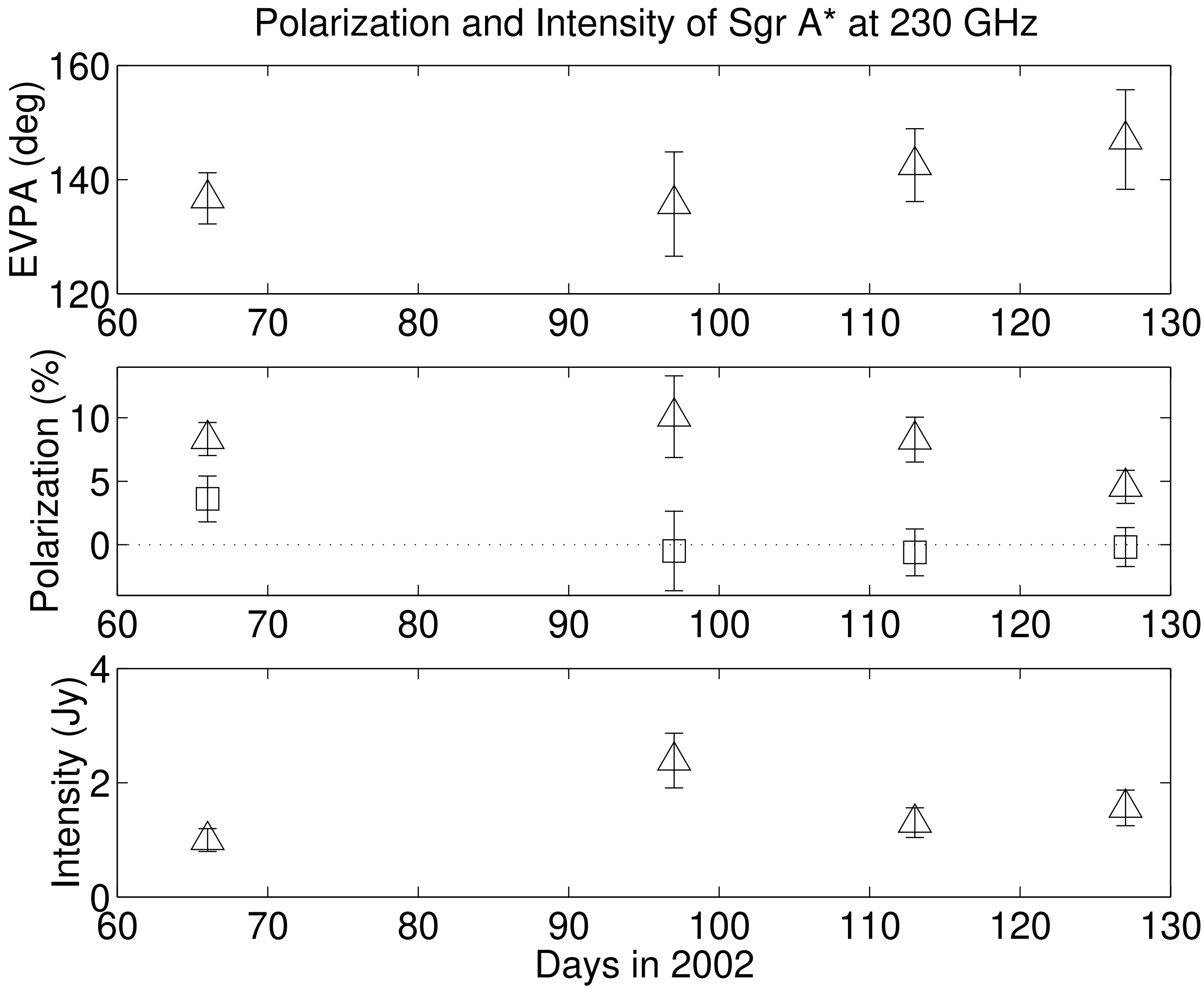

Fig. 3.— Lightcurves of the linear and circular polarization of Sgr A* as measured with BIMA at 230 GHz. In the upper panel, the electric vector position angle is plotted. In the middle panel, the fractional linear (triangles) and circular (squares) polarization is plotted. In the lower panel, the total intensity is plotted.

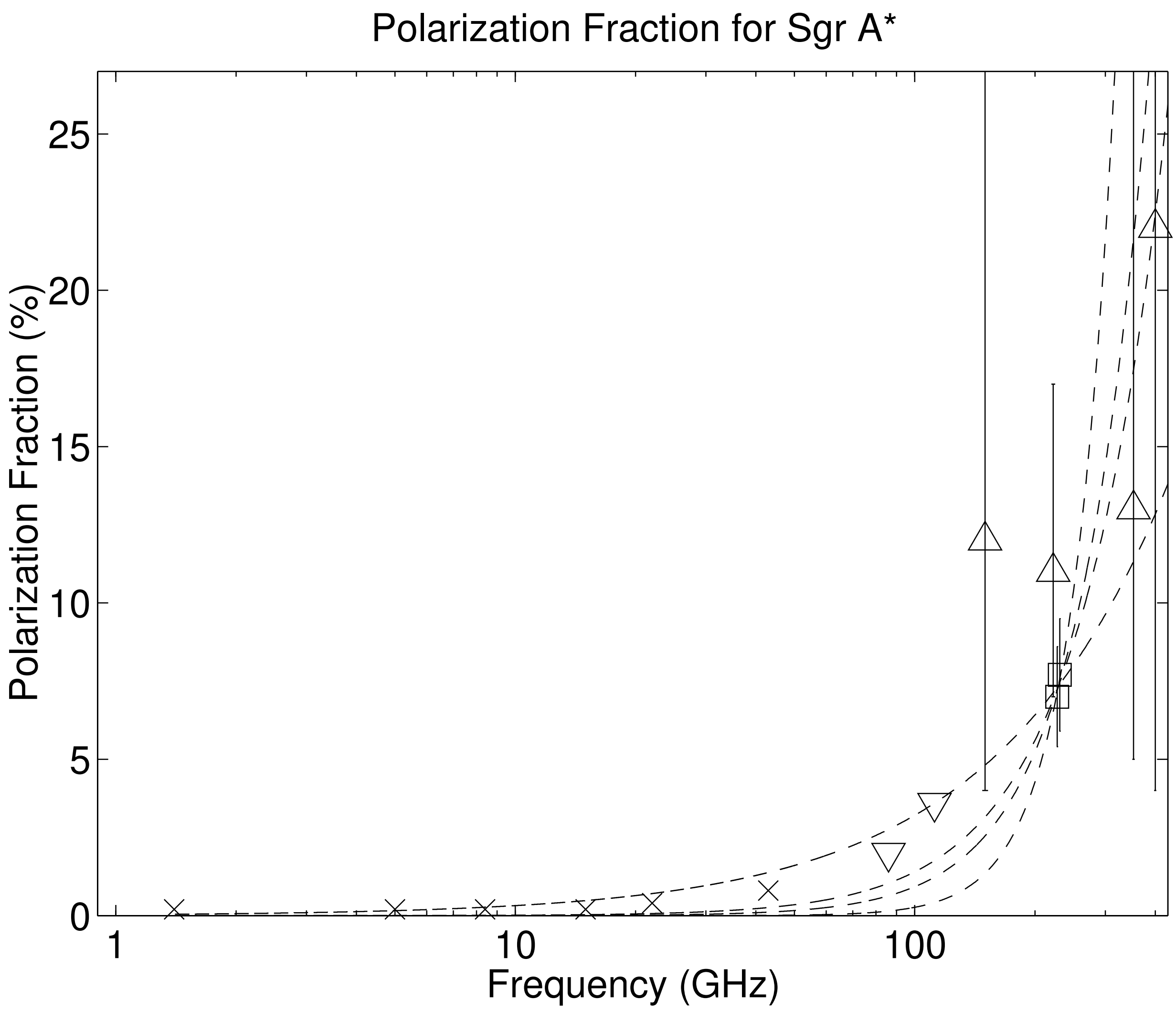

Fig. 4.— Polarization fraction as a function of frequency. Triangles are the A00 data. Squares are the new BIMA data. The inverted triangles are the 3 mm BIMA upper limits. Crosses are VLA upper limits. All error bars and upper limits are plotted at 2σ levels. The dashed lines are power law models for the polarization fraction with indices of 1.0, 2.0, 2.5 and 4.

Table 1. Polarimetric Observations of Sgr A*

Date	Array	b_{maj} ($''$)	b_{min} ($''$)	p.a. (deg)	τ_{230}^{zenith} (nepers)
02 March 2002	B	2.6	0.7	1.7	0.29
08 April 2002	C	6.5	1.7	9.4	0.78
24 April 2002	C	8.7	1.7	3.2	0.65
08 May 2002	C	6.6	1.8	8.7	0.36

Table 2. Polarized and Total Flux Density of Sgr A* at 230 GHz

Data Set	I (mJy)	Q (mJy)	U (mJy)	V (mJy)	p (%)	χ (deg)
ALL	1235 ± 24	12 ± 11	-88 ± 11	13 ± 14	7.2 ± 0.6	139 ± 4
LSB	1344 ± 26	10 ± 15	-93 ± 16	19 ± 19	7.0 ± 0.8	138 ± 5
USB	1165 ± 27	13 ± 15	-89 ± 16	-2 ± 18	7.7 ± 0.9	139 ± 5
B	999 ± 23	5 ± 13	-83 ± 13	36 ± 18	8.3 ± 0.9	137 ± 4
C	1483 ± 38	27 ± 16	-90 ± 17	0 ± 18	6.3 ± 0.8	143 ± 5
C1	2389 ± 89	6 ± 77	-241 ± 77	-12 ± 75	10.1 ± 2.3	136 ± 9
C2	1301 ± 59	28 ± 24	-104 ± 23	-8 ± 24	8.3 ± 1.3	143 ± 6
C3	1561 ± 45	29 ± 22	-65 ± 20	-3 ± 24	4.6 ± 0.9	147 ± 9